Appl Phys B (2010) 100: 759–764
DOI 10.1007/s00340-010-4032-8

**Applied Physics B**
**Lasers and Optics**

# Picosecond Nd:$BaY_2F_8$ laser discretely tunable around 1 μm

**A. Agnesi · F. Pirzio · G. Reali · A. Toncelli · M. Tonelli**

Received: 14 December 2009 / Revised version: 13 April 2010 / Published online: 6 May 2010
© Springer-Verlag 2010

**Abstract** Passive mode-locking of a diode-pumped Nd:$BaY_2F_8$ (Nd:BaYF) was achieved on four lines in the range 1040–1074 nm, employing a semiconductor saturable absorber mirror (SAM). Nearly Fourier-limited pulses with durations of 2.6 to 7.2 ps and output power ≈50 mW were generated in a dispersion-controlled resonator using a single prism for wavelength selection, tuning and dispersion management.

## 1 Introduction

Neodymium-doped fluoride crystals such as Nd:$YLiF_4$ (Nd:YLF) are excellent laser media for generation and amplification of short picosecond pulses in diode-pumped solid-state lasers at 1-μm wavelength [1–3]. Polarized emission as well as low thermal lensing allow the generation and the amplification of laser pulses with excellent spatial quality, only constrained by average power fracture limits lower than in more popular neodymium-doped oxides [4]. Since their fluorescence time of ∼500 μs is the longest among the class of neodymium-doped materials, they are also well suited for high-energy amplification of picosecond pulses at relatively low average power levels up to few watts.

While Nd:YLF is the most common fluoride material for 1-μm solid-state lasers, Nd:BaYF has recently been extensively investigated as an alternative medium with reduced fluorescence quenching and broader bandwidth [5–7]. Indeed, generation of mode-locking pulses as short as 3.5 ps has been recently reported [8], with a resonator employing an off-phase-matching second-harmonic crystal in order to suppress self-Q-switching instabilities.

In this work we further investigate picosecond pulse generation with Nd:BaYF and wavelength tunability, by taking a different approach. We designed a dispersion-compensated resonator with a simple, compact structure employing a single prism for both dispersion management and wavelength selection. Operating the laser in the soliton-like regime we achieved for the first time stable cw mode-locking with a shortest pulsewidth of 2.6 ps. No additional nonlinear crystals for inverse saturable absorption were used to stabilize the picosecond pulse regime against Q-switching as in [7, 8], where the resonator did not include spectral-selective and dispersive components.

Furthermore, the single-prism cavity readily allows wide tuning over several fluorescence peaks in the range 1040–1074 nm, with mode-locking pulsewidth ranging between 2.6 and 7.2 ps. This is an interesting option that, to our knowledge, was not previously investigated in diode-pumped neodymium lasers.

A numerical model was developed, showing that the single-prism angular dispersion allows one to stabilize mode-locking oscillation at each wavelength, whereas the negative group-velocity dispersion (GVD) helps minimize the pulse duration.

## 2 Experiments

The laser cavity setup for mode-locking experiments is shown in Fig. 1. The X-folded resonator was pumped by a $100 \times 1\ \mu m^2$ broad area emitter laser diode, with a maximum

A. Agnesi (✉) · F. Pirzio · G. Reali
INFN Sez. di Pavia and Dipartimento di Elettronica
dell'Università di Pavia, Via Ferrata 1, 27100 Pavia, Italy
e-mail: antonio.agnesi@unipv.it

A. Toncelli · M. Tonelli
CNR NEST and Dipartimento di Fisica dell'Università di Pisa,
Largo B. Pontecorvo, 3, 56127 Pisa, Italy

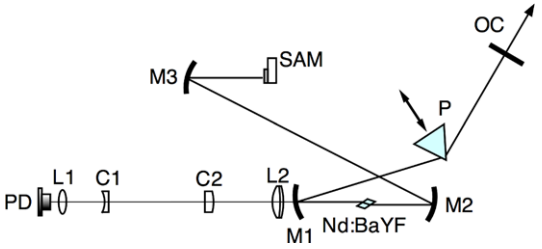


**Fig. 1** Resonator layout. PD: pump laser diode; L1: aspheric lens; L2: achromat lens; C1, C2: cylindrical lenses (15× telescope); M1, M2: concave mirrors, 100-mm curvature, HR at 1064 nm, high-transmissivity at 800–810 nm; M3: concave mirror, HR with 50-mm or 75-mm radius of curvature; P: FS or SF10 Brewster-cut prism; OC: output coupler mirror, 30′ wedge

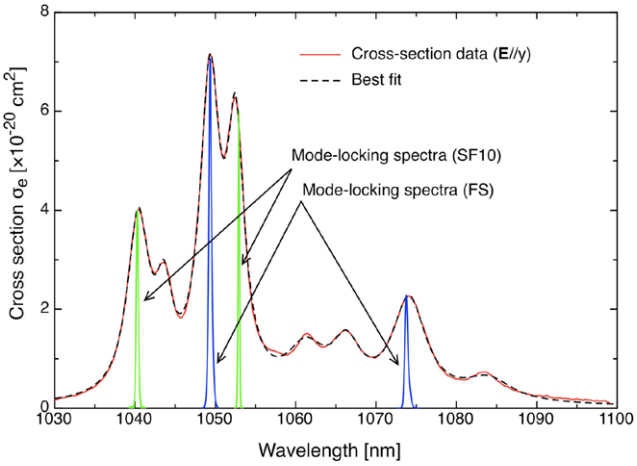


**Fig. 2** Fluorescence spectrum of Nd:BaYF at room temperature ($\mathbf{E}\|y$), fitted with 8 Lorentzian peaks. The results are summarized in Table 1. Also shown are the cw mode-locking spectra obtained either with FS single-prism (*blue curves*, centered at ≈1049 nm and ≈1074 nm) or SF10 single-prism (*green curves*, centered at ≈1040 nm and ≈1053 nm)

**Table 1** Results of fluorescence spectrum best fit with 8 Lorentzian peak functions, yielding for each central wavelength the maximum cross section and the FWHM

| $\sigma_e$ [$\times 10^{20}$ cm$^2$] | $\lambda_{peak}$ [nm] | $\Delta\lambda_{FWHM}$ [nm] |
|---|---|---|
| 3.6 | 1040.4 | 3.3 |
| 1.7 | 1043.6 | 2.5 |
| 6.2 | 1049.3 | 3.0 |
| 5.0 | 1052.5 | 2.6 |
| 0.94 | 1061.2 | 5.9 |
| 1.0 | 1066.3 | 4.4 |
| 2.0 | 1074.1 | 5.1 |
| 0.46 | 1083.9 | 7.2 |

output power of 1 W at 805 nm. It was collimated by an 8-mm focal aspheric lens L1, expanded by a factor 15 in the slow-axis direction with a cylindrical telescope (C1 and C2) and then focused in the Nd:BaYF sample by a 80-mm focal achromat L2. The pump spot size was measured in air with a CCD camera yielding a spot radius $W_x \times W_y \approx 36 \times 11$ μm$^2$ (intensity at $1/e^2$) along the (horizontal) slow- and fast-axis respectively. For this experiment we used the same 1.8% doped, 4-mm long Brewster-cut Nd:BaYF crystal employed in our earlier investigations [8]. The crystal was grown in a home-made Czochralski furnace with conventional resistive heating and equipped with an optical apparatus for real-time automatic diameter control system. The starting materials were supplied by AC Materials as 99.999% fluoride powders [5].

This sample was cut for propagation and polarization of the laser beam along the optical $(x, y, z)$ instead of crystallographic $(a, b, c)$ axes [9], in order to avoid the Lyot-filter effect due to the monoclinic crystal structure. The lifetime of the material is 470 μs at room temperature. The fluorescence peaks near 1 μm for this particular crystal orientation and field polarization ($\mathbf{E}\|y$) are shown in Fig. 2, while Table 1 summarizes emission cross section and linewidth of each peak modeled according to the Lorentzian distribution corresponding to homogeneous broadening.

Wavelength temperature tuning of the pump diode output allowed us to match the Nd:BaYF secondary absorption peak around 804 nm and obtain a maximum absorbed pump power of ≈590 mW. At such a low pump-power level, we operated without any crystal active cooling and, as expected, we did not experience any thermal problem during laser operation.

According to an ABCD modeling, the X-shaped resonator waist radius within the Brewster-oriented crystal was ≈70 × 37 μm$^2$. According to Fig. 1, the distances between cavity elements, were: M1–M2≈107 mm, M2–M3 = 350 mm, M1–P = 230 mm, P–OC = 110 mm. The distance M3–SAM was dependent on the M3 mirror radius of curvature: it was ≈24 mm in case of 50-mm radius of curvature and ≈34 mm in case of 75-mm radius of curvature. We tested SAMs with either 1% or 2% nominal absorption (BATOP GmbH), while the output coupler (OC) transmissivity was $T_{oc} = 0.4\%$.

For wavelength selection and intracavity dispersion compensation, a single Brewster-cut prism was employed, either SF10 or Fused Silica (FS). Beside a reduction in cavity footprint and complexity, the single-prism configuration allows an easy wavelength tuning by simply angular alignment of the OC. Additionally, it is known that negative GVD can be introduced with such a single-prism configuration [10], which can be interesting to minimize the pulse width in combination with the self-phase-modulation yielded by the gain medium.

At first we tested a cavity setup employing a 2% nominal absorption SAM and a FS prism. In this configuration cw mode-locking was achieved only for two different

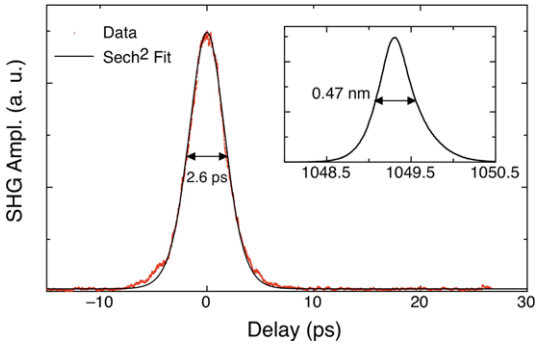


**Fig. 3** Shortest autocorrelation pulses at ≈1049 nm and the corresponding spectrum. The 1% SAM and the FS prism were employed in this setup

wavelengths. At the central wavelength of 1049.6-nm, 3.5-ps-long pulses with a 0.53-nm FWHM wide optical spectrum were measured, while at 1074-nm, 0.9-nm FWHM wide spectra yielded 2.7-ps-long pulse trains. The average output power was in both cases ≈30 mW and the repetition rate was ≈180 MHz. It is worth noticing that a tight focusing of the cavity mode (M3 = 50-mm radius of curvature) at the SAM was necessary to stabilize the mode-locking regime. In these conditions stability was limited to only a few minutes due to SAM optical damage.

In order to reduce the threshold for cw mode-locking and reduce damage risk, we substituted the 2% SAM with a second device with 1% nominal absorption and replaced the 50-mm radius of curvature mirror with a 75-mm one. Stable mode-locking operation was readily observed both at 1049.4 nm and at 1073 nm. In Fig. 3 the shortest pulses autocorrelation trace and optical spectrum are shown. We obtained 50-mW average output power, either with 2.6-ps-long pulses at 1049.4 nm or 4.4-ps-long pulses at 1074 nm. In all cases the pulses were nearly Fourier-limited, with duration × bandwidth products approaching the limit for $sech^2$ pulse shape (≈0.32) for the shortest pulse measured.

Moreover, employing a more dispersive SF10 prism instead of the FS prism, we improved the angular spectral selectivity of the resonator. Under these new conditions it was possible to obtain stable mode-locking also at 1040 nm and at 1053 nm with 7.2-ps-long pulses in both cases (Fig. 2). Neither mode-locking nor even lasing could be achieved at other fluorescence peaks owing to small cross sections or to competition with close stronger laser transitions.

For completeness we note that the resonator with no intracavity prism was not successful in generating a stable cw mode-locking train: damage of the SAM due to Q-switched mode-locking was frequently observed instead.

**Table 2** Parameters used in the numerical model

| Parameter | Value |
|---|---|
| Nd:BaYF saturation fluence $F_{SG}$ at 1049 nm | 3.1 J/cm$^2$ |
| Mode radius $w_G$ in Nd:BaYF | 30 μm |
| Nd:BaYF refraction index $n_G$ | 1.51 |
| Nd:BaYF saturation energy $E_{SG} = F_{SG}\pi n_G w_G^2$ | 132 μJ |
| Crystal length $l_G$ | 4 mm |
| SAM saturation fluence $F_{SA}$ | 70 μJ/cm$^2$ |
| SAM recovery time $\tau_A$ | 2 ps |
| Spot radius $w_A$ on SAM | 20–30 μm |
| SAM saturation energy $E_{SA} = F_{SA}\pi w_A^2$ | 2–0.9 nJ |
| SAM modulation $\Delta R$ (saturable/non-saturable) | 0.6/0.4% |
| Passive loss $L$, including SAM's non-saturable absorption | 1% |
| Output coupling $T_{oc}$ | 0.4% |
| Round-trip time $T_R$ | 5.5 ns |

## 3 Numerical modeling

The threshold for stable cw mode-locking in the non-dispersive picosecond regime is given by [11]

$$P_{out,th} = \frac{T_{oc}}{T_R}\sqrt{\Delta R E_{SA} E_{SG}} \tag{1}$$

where $T_{oc}$ is the output coupler transmissivity, $T_R$ the round-trip time, $E_{SA}$ and $E_{SG}$ the saturation energy of the SAM and of the Nd:BaYF, respectively.

In our setup, using the parameters summarized in Table 2, this condition should be always fulfilled at the strongest transition near 1049 nm, and at least with the 1% SAM at 1074 nm. Nevertheless, we did not succeed in achieving cw mode-locking without the intracavity prism.

However, since the shortest pulses compatible with these gain bandwidths are intermediate between a basically non-dispersive regime (few picosecond duration) and highly-dispersive <100-fs typical duration, in order to gain further insights into the laser operation, we developed a numerical model of the passively mode-locked dispersive oscillator. The laser gain was modeled as a homogeneously-broadened

$$g = \frac{g_0}{1 + 2E/(T_R P_{SG})} \tag{2}$$

$$E = \int_{-\infty}^{+\infty} |A(t)|^2 \, dt \tag{3}$$

$g_0$ being the single-pass small-signal gain, $P_{SG} = E_{SG}/T_R$ the saturation power and $A(t)$ the pulse amplitude. $P(t) = |A^2(t)|$ is the instantaneous power and $E$ is the pulse energy. The SAM was assumed as a saturable absorber with single-

exponential time decay time constant $\tau_A$ and initial loss $q_0$. Its dynamics is described by the equation

$$\frac{dq}{dt} = -\frac{q - q_0}{\tau_A} - q\frac{P(t)}{E_{SA}} \tag{4}$$

which can readily be integrated:

$$q(t) = q_0\left\{1 + \frac{1}{\tau_A}\int_{-\infty}^{t} du \exp\left[\frac{u}{\tau_A} + \frac{E(u)}{E_{SA}}\right]\right\} \times \exp\left[-\frac{t}{\tau_A} - \frac{E(t)}{E_{SA}}\right] \tag{5}$$

$$E(t) = \int_{-\infty}^{t} P(u)\, du \tag{6}$$

Second-order dispersion effects ($D$) as well as gain dispersion and shaping (linewidth $\Delta\omega_G$) [12] were conveniently modeled in the frequency space with the fast-Fourier transform:

$$\hat{A}'(\omega) = \exp\left[\frac{g}{2}\frac{1}{1 + i(2\omega/\Delta\omega_G)}\right]\exp\left(-i D\omega^2\right)\hat{A}(\omega) \tag{7}$$

In our notation $A$ and $A'$ correspond to the pulse amplitude (or its Fourier transform) respectively before and after each particular element affecting either the amplitude or the phase of the intracavity pulse.

The effect of linear and nonlinear loss components, as well as the self-phase-modulation (through the nonlinear index $n_2$ over the laser crystal of length $l_G$) were best modeled in the time domain:

$$A'(t) = [1 - L - T_{OC}]^{1/2} A(t) \tag{8}$$

$$A'(t) = \left[1 - q(t)\right]^{1/2} A(t) \tag{9}$$

$$A'(t) = \exp\left[i\frac{2\pi n_2 l_G}{\lambda} I(t)\right] A(t) \tag{10}$$

the pulse intensity being

$$I(t) = \frac{2|A^2(t)|}{\pi n_G w_G^2} \tag{11}$$

We concentrated on the setup yielding the shortest pulse duration, near the main 1049-nm peak, with the 1% SAM. Figure 4 shows the dependence of pulse width on the net intracavity dispersion, for different values of nonlinear index $n_2$ and available bandwidth.

The nonlinear index required to reproduce the experimental results seems comparable to that of Nd:YLF ($n_2 \approx 1.4 \times 10^{-16}$ cm$^2$/W [13]).

We notice that the best agreement between the numerical and the experimental results was achieved by assuming an effective linewidth of ≈80% of the full bandwidth at 1049 nm, with net GVD $< -1000$ fs$^2$ (FS prism). However, modeling the resonator with the real double-peaked

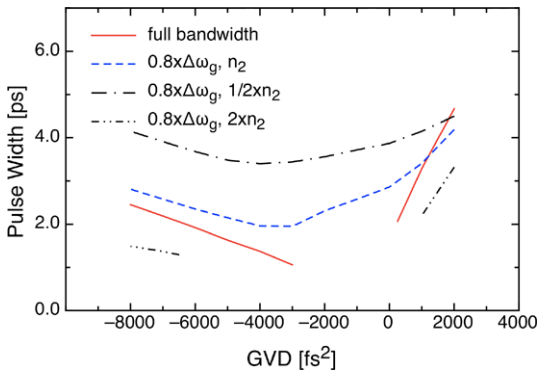


**Fig. 4** Numerical results: pulse duration as a function of the total intracavity dispersion with spot size $w_A = 30$ μm at the SAM, with either full fluorescence spectrum available or 80% of the main peak at 1049 nm. The value $n_2 = 1.4 \times 10^{-16}$ cm$^2$/W of Nd:YLF was used for reference

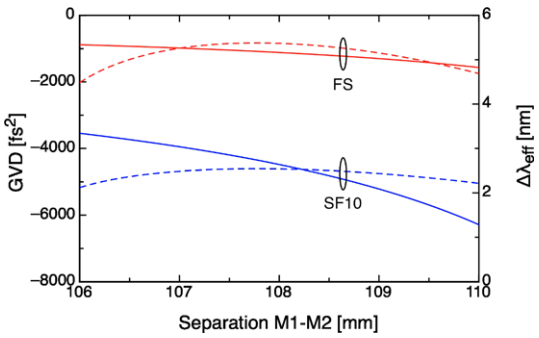


**Fig. 5** Net (total) intracavity GVD dispersion with FS and SF10 prisms (*continuous lines*), as well as the effective resonator bandwidth owing to the prism angular dispersion (*dashed lines*), assuming $\varepsilon = 1.4\%$

gain profile at 1049, 1053 nm as in Fig. 2, with no additional bandwidth-limiting components, we found that stable mode-locking was not allowed in the net dispersion range $-3000$ fs$^2$ $<$ GVD $<$ $+250$ fs$^2$. In particular, without the intracavity prism the total (positive) dispersion of the cavity is very likely in this instability range. Furthermore, the shortest pulses ≈1.0 ps should be generated at 1049 nm if sufficient negative dispersion were introduced with no bandwidth-limiting effects at least over the double-peak range of ∼8 nm. Also, one might consider to increase the positive dispersion in order to generate strongly chirped, compressible picosecond pulses as it is pursued in high-power ultrafast ytterbium oscillators, for example [14].

While we assumed the unknown GVD contribution of Nd:BaYF comparable to ∼20 fs$^2$/mm of the better characterized Nd:YLF [15], this is not a critical parameter since the negative GVD yielded by the prism arrangement is surely much higher.

Figure 5 shows the net dispersion of the resonator with the single prism, as calculated with ABCD ray tracing as in [10] at different M1–M2 mirror separations. Addition-

ally, the effective bandwidth $\Delta\lambda_{eff}$ of the single-prism dispersive resonator was roughly estimated requiring that the transverse shift $\delta = (dx/d\lambda)\Delta\lambda$ of the mode axis in the laser crystal at $\lambda + \Delta\lambda$ produce a round-trip maximum gain reduction comparable to the total resonator loss $\varepsilon = L + T_{oc}$, owing to the Gaussian pump distribution along the transverse $x$-axis $\sim \exp[-2(x/w_G)^2]$:

$$1 - \exp\left[-(\delta/w_G)^2\right] \sim \varepsilon \tag{12}$$

$$\Delta\lambda_{eff} \sim \frac{2\sqrt{\varepsilon}}{|dx/d\lambda|} w_G \tag{13}$$

It is worth noting that this criteria is basically analogous to that for the angular misalignment tolerance introduced by Hauck et al. [16], with the exception that the relevant loss increment $\varepsilon$ to be considered in these cw lasers is generally smaller than 10%.

The effective resonator bandwidth estimated for both the prism glasses accounts reasonably well for the wavelength selectivity observed experimentally. Indeed, the FS prism was unable to isolate the 1053-nm mode-locking spectrum, which was significantly disturbed by the competition with the line at 1049 nm having higher gain cross section. This suggests that the FS prism yielded sufficient effective bandwidth to allow generation of shorter pulses: indeed, with an almost identical Nd:phosphate glass laser setup employing a single FS prism we observed pulses as short as 150-fs with 8.5-nm bandwidth. Therefore, while the minimum pulse width of 1.0 ps predicted by the model for this Nd:BaYF laser seems perfectly reasonable given the fluorescence bandwidth of 3 nm at 1049 nm, it is possible that it cannot be reached actually owing to some other effect specifically related to the crystal itself. For example, we note that using a much brighter single-mode beam to pump Nd:YLF and Nd:LSB lasers with comparable wide bands, the pulse width was found to be nearly twice as short compared to direct multimode diode-pumping [17]: clearly this depends on the overlap between pump and resonant beams within the absorption length of the crystal [18], which in our case is relatively poor (low-absorbing crystal).

Finally, it is worth noting that the separation of the prism and the "virtual" second prism [10] in the experiment was as large as 50–75 cm, yielding a GVD $< -1000$ $fs^2$ (FS prism) or $< -6000$ $fs^2$ (SF10 prism). This was achieved with a most compact setup, as one may readily appreciate from Fig. 1: a traditional two-prism resonator would have required a dispersive arm up to ≈3 times longer.

## 4 Conclusions

A passively mode-locked picosecond diode-pumped $Nd^{3+}$-fluoride laser tunable at four distinct wavelengths in the range 1040–1074 nm has been reported for the first time to our knowledge. The remarkable tuning range of ≈34 nm for passive mode-locking operation in Nd:BaYF is quite unique among the most common neodymium-doped lasers [19–21], and is related to the particular fluorescence spectrum associated to the $^4F_{3/2} \rightarrow {}^4I_{11/2}$ transitions with $\mathbf{E} \| y$, with several peaks of comparable strength.

Fourier-limited pulses as short as 2.6 ps have been generated in Nd:BaYF for the first time. This might be interesting for mixing synchronous mode-locked lasers with wavelength separation of few nanometers for the generation of THz radiation in nonlinear crystals [22].

For efficient nonlinear optical applications, such a low-power oscillator might be readily used with either bulk Nd:BaYF amplifiers or even fiber amplifiers, scaling the pulse energy in the multi-μJ range.

A numerical model yields a satisfactory interpretation of the experimental observations with the single-prism dispersive resonator. In particular, it was shown that prism angular dispersion limits the bandwidth allowing to stabilize effectively the mode-locking at each fluorescence peak wavelength, while the negative GVD obtained with the proposed setup minimizes the pulse duration.

## References


1. G.P.A. Malcolm, P.F. Curley, A.I. Ferguson, Opt. Lett. **15**, 1303 (1990)
2. U. Keller, T.H. Chiu, J.F. Ferguson, Opt. Lett. **18**, 217 (1993)
3. K.J. Snell, D. Lee, K.F. Wall, P.F. Moulton, in *Advanced Solid State Lasers*, ed. by H. Injeyan, U. Keller, C. Marshall. Trends in Optics and Photonics Series, vol. 34 (Optical Society of America, Washington, 2000), pp. 55–59
4. W. Koechner, *Solid State Laser Engineering*, 6th edn. (Springer, Berlin, 2006)
5. A. Agnesi, A. Guandalini, G. Reali, E. Sani, A. Toncelli, M. Tonelli, IEEE J. Quantum Electron. **39**, 971 (2003)
6. A. Agnesi, G. Carraro, A. Guandalini, G. Reali, E. Sani, A. Toncelli, M. Tonelli, Opt. Express **12**, 3765 (2004)
7. A. Agnesi, A. Guandalini, A. Tomaselli, E. Sani, A. Toncelli, M. Tonelli, Opt. Lett. **29**, 1638 (2004)
8. A. Agnesi, F. Pirzio, G. Reali, A. Toncelli, M. Tonelli, H.P. Jenssen, Opt. Commun. **281**, 6094 (2008)
9. J.J. Owen, A.K. Cheetham, R.A. McFarlane, J. Opt. Soc. Am. B **15**, 684 (1998)
10. D. Kopf, G.J. Spühler, K.J. Weingarten, U. Keller, Appl. Opt. **35**, 912 (1996)
11. C. Hönninger, R. Paschotta, F. Morier-Genoud, M. Moser, U. Keller, J. Opt. Soc. Am. B **16**, 46 (1999)
12. H.H. Haus, J. Appl. Phys. **46**, 3049 (1975)
13. B. Braun, K.J. Weingarten, F.X. Kärtner, U. Keller, Appl. Phys. B **61**, 429 (1995)
14. G. Palmer, M. Emons, M. Siegel, A. Steinmann, M. Schultze, M. Lederer, U. Morgner, Opt. Express **15**, 16017 (2007)
15. N.P. Barnes, D.J. Gettemy, J. Opt. Soc. Am. **70**, 1244 (1980)
16. R. Hauck, H.P. Kortz, H. Weber, Appl. Opt. **19**, 598 (1980)
17. U. Keller, K.J. Weingarten, F.X. Kärtner, D. Kopf, B. Braun, I.D. Jung, R. Fluck, C. Hönninger, N. Matuschek, J. Aus der Au, IEEE J. Sel. Top. Quantum Electron. **2**, 435 (1996)

18. D. Kopf, K.J. Weingarten, L.R. Brovelli, M. Kamp, U. Keller, Opt. Lett. **19**, 2143 (1994)
19. S. Kück, L. Fornasiero, E. Mix, G. Huber, Appl. Phys. B **67**, 151 (1998)
20. L. Fornasiero, S. Kück, T. Jensen, G. Huber, B.H.T. Chai, Appl. Phys. B **67**, 549 (1998)
21. L. Fornasiero, T. Kellner, S. Kück, J.P. Meyn, P.E.-A. Möbert, G. Huber, Appl. Phys. B **68**, 67 (1999)
22. D. Creeden, J.C. McCarthy, P.A. Ketteridge, P.G. Schunemann, T. Southward, J.J. Komiak, E.P. Chiklis, Opt. Express **15**, 6478 (2007)